ACS chemical biology

Articles

pubs.acs.org/acschemicalbiology

Discovery of PTPRJ Agonist Peptides That Effectively Inhibit *in Vitro* Cancer Cell Proliferation and Tube Formation

Francesco Ortuso,[†,#] Francesco Paduano,[‡,#] Alfonso Carotenuto,[§,#] Isabel Gomez-Monterrey,[§] Anna Bilotta,[‡] Eugenio Gaudio,[‡,∥] Marina Sala,[§] Anna Artese,[†] Ermelinda Vernieri,[⊥] Vincenzo Dattilo,[‡] Rodolfo Iuliano,[‡] Diego Brancaccio,[§] Alessia Bertamino,[⊥] Simona Musella,[⊥] Stefano Alcaro,[†] Paolo Grieco,[§] Nicola Perrotti,[‡] Carlo M. Croce,[∥] Ettore Novellino,[§] Alfredo Fusco,[¶] Pietro Campiglia,*[,⊥] and Francesco Trapasso*[,‡]

[†]Dipartimento di Scienze della Salute and [‡]Dipartimento di Medicina Sperimentale e Clinica, Università "Magna Græcia" di Catanzaro, Campus "S. Venuta", 88100 Catanzaro, Italy

[§]Dipartimento di Farmacia, Università degli Studi di Napoli "Federico II", 80131 Napoli, Italy

[∥]Department of Molecular Virology, Immunology and Medical Genetics and Comprehensive Cancer Center, The Ohio State University, Columbus, Ohio 43210, United States

[⊥]Dipartimento di Farmacia, Università di Salerno, 84084 Fisciano, Italy

[¶]Dipartimento di Biologia e Patologia Cellulare e Molecolare c/o Istituto di Endocrinologia ed Oncologia Sperimentale del CNR, Università degli Studi di Napoli "Federico II", 80131 Napoli, Italy

Supporting Information

ABSTRACT: PTPRJ is a receptor protein tyrosine phosphatase involved in both physiological and oncogenic pathways. We previously reported that its expression is strongly reduced in the majority of explored cancer cell lines and tumor samples; moreover, its restoration blocks *in vitro* cancer cell proliferation and *in vivo* tumor formation. By means of a phage display library screening, we recently identified two peptides able to bind and activate PTPRJ, resulting in cell growth inhibition and apoptosis of both cancer and endothelial cells. Here, on a previously discovered PTPRJ agonist peptide, PTPRJ-pep19, we synthesized and assayed a panel of nonapeptide analogues with the aim to identify specific amino acid residues responsible for peptide activity. These second-generation nonapeptides were tested on both cancer and primary endothelial cells (HeLa and HUVEC, respectively); interestingly, one of them (PTPRJ-19.4) was able to both dramatically reduce cell proliferation and effectively trigger apoptosis of both HeLa and HUVECs compared to its first-generation counterpart. Moreover, PTPRJ-pep19.4 significantly inhibited *in vitro* tube formation on Matrigel. Intriguingly, while ERK1/2 phosphorylation and cell proliferation were both inhibited by PTPRJ-pep19.4 in breast cancer cells (MCF-7 and SKBr3), no effects were observed on primary normal human mammary endothelial cells (HMEC). We further characterized these peptides by molecular modeling and NMR experiments reporting, for the most active peptide, the possibility of self-aggregation states and highlighting new hints of structure−activity relationship. Thus, our results indicate that this nonapeptide might represent a great potential lead for the development of novel targeted anticancer drugs.

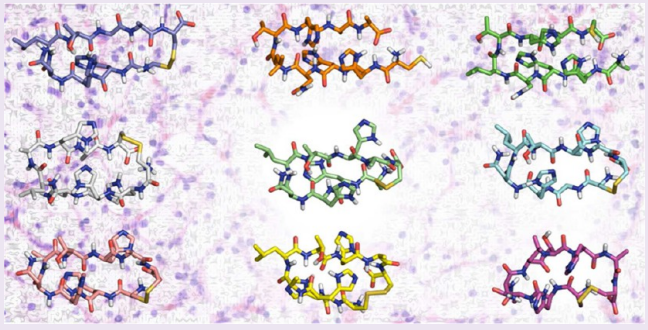

The balanced activity of protein tyrosine kinases (PTKs) and protein tyrosine phosphatases (PTPs) governs the global state of tyrosine phosphorylation in the cell, thus modulating important signaling pathways such as cell proliferation, adhesion, and migration. Mutations or overexpression of PTKs that modify their normal activity often result in malignant transformation;[1] for this reason, small molecules or monoclonal antibodies able to inhibit PTKs activity are well-established anticancer drugs.[2,3] In this context, PTPs that antagonize the oncogenic PTKs signaling are considered potential tumor suppressors and, consequently, potential targets for novel anticancer therapies.[4] PTPRJ (also known as DEP-1, HPTPeta, or CD148) is a receptor-type protein tyrosine phosphatase[5,6] of particular interest for its role in human and experimental tumorigenesis.[7] Indeed, even though PTPRJ aberration is not an early event in tumorigenesis,[8,9] its tumor suppressor activity in several models of mammary, thyroid, colon, and pancreatic cancers was clearly established by numerous studies.[10−15] In addition, numerous reports showed that many players of the mitogenic signal are negatively influenced by PTPRJ in both normal and cancer cells. In fact, PTPRJ was demonstrated

Received: December 24, 2012
Accepted: April 29, 2013
Published: April 29, 2013

Table 1. Structure, Analytical Data, and Percent of Growth Inhibition on HeLa cells Treated with 160 μM PTPRJ pep-19 Analogues (PTPRJ pep-19.0-19.8)

			ESI MS		% of cell growth inhibition[b]		
PTPRJ peptides	sequence	HPLC k'[a]	found	calcd	24 h	48 h	72 h
19	[CHHNLTHAC]	3.34	1931.16	1033.5		4.5 ± 0.1.4	19 ± 2.82
19.0	CHHNLTHAC	3.28	1035.1	1035.7			4 ± 1.4
19.1	**A**HHNLTHAC	3.22	1003.1	1003.7			
19.2	[C**A**HNLTHAC]	3.56	967.1	967.6	16.5 ± 2.12	30 ± 2.82	32.0 ± 4.2
19.3	[CHA**N**LTHAC]	3.56	967.1	967.4	28 ± 5.5	46 ± 4.2	51 ± 1.4
19.4	[CHH**A**LTHAC]	3.44	990.1	990.4	48.0 ± 2.82	62.5 ± 4.9	66.5 ± 2.12
19.5	[CHHN**A**THAC]	3.26	991.0	991.4		2 ± 1.5	19 ± 4.2
19.6	[CHHNL**A**HAC]	3.45	1003.1	1003.2			19 ± 4.2
19.7	[CHHNLT**A**AC]	3.56	967.1	967.6		4.5 ± 2.13	20 ± 1.4
19.8	CHHNLTHA**A**	3.22	1003.1	1003.5			

[a] k' = [(peptide retention time solvent retention time)/solvent retention time]. [b] The relative cell growth was expressed as a percentage of the growth observed in untreated cells at 24, 48, and 72 h. The results are presented as mean values ± SD of at least three independent experiments.

to be able to dephosphorylate and inactivate several receptor tyrosine kinases (RTKs), including PDGFR,[16] HGFR,[17] RET,[18] and EGFR,[19] whose aberration in cancer cells is accountable for self-sufficiency cell growth, the first hallmark of cancer.[20] Noteworthy, another RTK inhibited by PTPRJ is VEGFR2,[21] whose activity is necessary for the formation of new vessels in tumor progression (angiogenesis), another hallmark of cancer.[20] All of these findings make PTPRJ a fascinating candidate for the ideation of innovative therapeutic strategies. To this end, Takahashi et al.[22] successfully used a PTPRJ monoclonal antibody able to induce ERK1/2 dephosphorylation and inhibition of both *in vitro* cell growth and *in vivo* angiogenesis.

In this context and as part of a wide research program aimed to the identification of new PTPRJ-targeted anticancer agents, we recently described the isolation and characterization of synthetic PTPRJ-binding peptides from a combinatorial phage display library.[23] *In vitro*, two of these peptides (PTPRJ-pep19 and PTPRJ-pep24) were shown to be responsible for both biochemical and biological PTPRJ-mediated effects. In fact, the administration of both PTPRJ-19 ([^{1}Cys-^{2}His-^{3}His-^{4}Asn-^{5}Leu-^{6}Thr-^{7}His-^{8}Ala-^{9}Cys]-OH) and PTPRJ-pep24 ([^{1}Cys-^{2}Leu-^{3}His-^{4}His-^{5}Tyr-^{6}His-^{7}Gly-^{8}Ser-^{9}Cys]-OH) peptides to human cervical HeLa cancer cell line and human umbilical vein endothelial cells (HUVECs) dramatically reduced the extent of both MAPK phosphorylation, a critical mediator of mitogenic signals, and total phospho-tyrosine levels and, conversely, induced a significant increase of the cell cycle inhibitor p27^{Kip1}. Moreover, these PTPRJ agonist peptides both reduce proliferation and trigger apoptosis of treated cells.[23]

In the present study, we considered PTPRJ-pep19 as a valuable starting point for the development of a novel class of potential chemotherapeutic agents. Here, we demonstrate that PTPRJ-pep19.4, a derivative of PTPRJ-pep19 generated through an Ala-scan analysis, was able to (a) reduce the phosphorylation of ERK1/2; (b) inhibit HeLa cancer cell proliferation, and (c) trigger apoptosis in a much more efficient way than its lead compound. HUVEC cell proliferation was also inhibited by PTPRJ-pep19.4, although to a lower extent compared to HeLa cells. Moreover, PTPRJ-pep19.4 effectively blocked *in vitro* HUVEC tube formation. Our results strongly encourage the pursuit of this path for the development of a novel class of targeted anticancer drugs.

RESULTS AND DISCUSSION

PTPRJ Ala-scan Peptide Derivatives Inhibit HeLa Cancer Cell Proliferation. Through a phage display library screening, we recently identified two nonapeptides (named PTPRJ-pep19 and -pep24) with the ability to bind and trigger PTPRJ activity; these peptides could induce MAPK dephosphorylation and inhibit cell growth of HeLa and HUVEC cells, although to a low extent.[23] Here, in order to generate PTPRJ peptide agonists with improved biological activity, we (a) investigated the role of the peptide circularization, synthesizing a PTPRJ-pep19 derivative deprived of the disulfide bridge between the first and the last cysteine residues, and then (b) pursued an Ala-scan procedure consisting in the systematic substitution of each PTPRJ-pep19 residue with a L-alanine (Table 1).

This latter approach resulted in the generation of a panel of nine peptides, named PTPRJ-pep19.0 to -pep19.8. All new derivatives were tested in HeLa cancer cells for the assessment of their ability to inhibit cell proliferation; cells were treated with 160 μM concentration of each compound, and cell count was performed 24, 48, and 72 h after treatment. Interestingly, PTPRJ-pep19.4 was responsible for a reduction of cell proliferation up to 66.5% versus 20% of PTPRJ-pep19 (Figure 1). Values of cell growth inhibition for all tested peptides in this experiment are reported in Table 1.

The above-reported data suggested important structure–activity relationships for this small library of derivatives. First, the disulfide bridge appears to have effect upon cell growth inhibition as demonstrated by our previous work.[23] In fact, all three linear compounds used, namely, PTPRJ-pep19.0 (that only differs from PTPRJ-pep19 for the absence of the disulfide bridge) and PTPRJ-pep19.1 and -pep19.8 (which incorporate an Ala residue at position 1 and 9, respectively), lost their ability to activate PTPRJ (Table 1). Second, the most interesting result was obtained with peptides modified at the PTPRJ-pep19 N-terminus. In fact, the substitution of ^{3}His or ^{4}Asn into the cyclic PTPRJ-pep19 by Ala produced a dramatic increase in the biological activity of the corresponding analogues (PTPRJ-pep19.3 or -pep19.4), resulting in a cell growth inhibition ranging from two to three times higher compared to their lead compound. In particular, the observed effect was time-dependent, generating a 48%, 62.5%, and 66.5% reduction of HeLa cell number at 24, 48, and 72 h, respectively. These data suggest that either a lack of polar side chains in these positions or the introduction of low hindrance, lipophilic features is well accepted. Finally, the substitution of ^{5}Leu or ^{6}Thr or ^{7}His residues by Ala (PTPRJ-pep19.5, -pep19.6, and -pep19.7) did not modify the weak cell growth inhibition levels exhibited by PTPRJ-pep19.

To demonstrate PTPRJ-pep19.4/PTPRJ interaction in living cells, we transfected *Ptprj*-negative NIH3T3 cells with a vector containing a *PTPRJ* cDNA (Figure S1A in Supporting Information),

dx.doi.org/10.1021/cb3007192 | ACS Chem. Biol. 2013, 8, 1497–1506

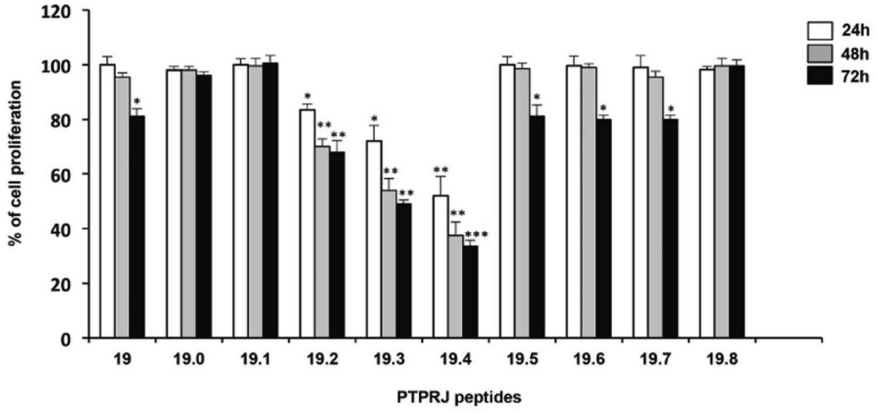

Figure 1. Cell growth inhibition induced by PTPRJ peptides in HeLa cells. Relative cell growth (as a percentage of the growth observed in untreated cells) at different intervals of treatments (from 24 to 72 h) is reported. HeLa cells were treated once with PTPRJ peptides for 24 h (white columns) or treated every 24 h for 48 h (gray columns) and for 72 h (black columns). Results represent the mean ± SD of three independent experiments. $*P < 0.05$, $**P < 0.01$, $***P < 0.001$ compared to untreated cells by unpaired two-tailed Student's t test.

as reported in our previous paper.[23] PTPRJ-transfected cells have been treated with a FITC-conjugated PTPRJ-pep19.4 peptide at growing amounts; mean fluorescence was then measured by flow cytometric analysis. Binding of PTPRJ-pep19.4 to PTPRJ was direct and dependent on PTPRJ expression; in fact, no binding was observed in NIH3T3 cells transfected with empty vector, indicating that PTPRJ-pep19.4 was specific for PTPRJ (Figure S1B in Supporting Information).

Ala-scan PTPRJ-pep19 Derivatives Negatively Modulate ERK1/2 Phosphorylation and Induce Apoptosis of HeLa Cancer Cells. According to our recent published results,[23] treatment of HeLa cells with 160 μM PTPRJ-pep19 resulted in a dramatic reduction of the ERK1/2 phosphorylation; the dephosphorylation effect reported in our previous investigation was rapid and transient and reached its peak within 15 min after treatment. In order to test the effects of the newly Ala-scan generated derivatives on ERK1/2 phosphorylation, we used the same approach as previously reported.[23] HeLa cells were treated with 160 μM concentration of the most potent antiproliferative compounds described in the previous section (PTPRJ-pep19.2, -pep19.3, and -pep19.4). As shown in Figure 2A, PTPRJ-pep19.2 and -pep19.3 reduced the ERK1/2 phosphorylation extent in a short term; these results are comparable to those observed with their precursor. Interestingly, the treatment with PTPRJ-pep19.4 induced a time-dependent reduction of ERK1/2 phosphorylation that reached its maximum at 60 min. ERK1/2 phosphorylation was also assessed 12, 24, and 48 h after PTPRJ-pep19.4 treatment of HeLa cells; as shown in Figure 2B, we observed a slight reduction of ERK1/2 phosphorylation extent in all cases. To further expand the concept of functional specificity of the PTPRJ-pep19.4/PTPRJ interaction, we knocked-down endogenous PTPRJ protein with specific siRNAs in HeLa cells. Forty-eight hours after transfection, cells were treated with either PTPRJ-pep19.4 and scramble peptide, and 1 h later we evaluated the ERK1/2 phosphorylation extent. Interestingly, ERK1/2 phosphorylation of PTPRJ knocked-down cells treated with PTPRJ-pep19.4 was higher compared to control treated with PTPRJ-pep19.4 alone, suggesting that ERK1/2 dephosphorylation is mediated by the PTPRJ protein levels (Figure 2C).

We also evaluated cell cycle perturbations induced by PTPRJ-pep19.2, -pep19.3, and -pep19.4 peptides on HeLa cells. Twenty-four hours after treatment, cells were collected and investigated by flow cytometric analysis; in Figure 2D is indicated the percentage of a sub-G1 population, suggestive of apoptotic cell death (see also Figure S2A in Supporting Information). Interestingly, while the administration of PTPRJ-pep19.2 was able to trigger cell death only in 6.1% of cell population, HeLa cells treated with PTPRJ-pep19.3 and -pep19.4 showed a 17.5% and 27,3% of dead cells, respectively. Apoptosis was confirmed by TUNEL assay (Figure S2B in Supporting Information).

PTPRJ-pep19.4 Partly Inhibits Cell Proliferation of HUVECs and Blocks *in Vitro* Tube Formation. In order to investigate the biological effects of PTPRJ-pep19.4 on normal endothelial cells, HUVECs were treated with 160 μM peptide. Similarly to what observed with HeLa cells, PTPRJ-pep19.4 significantly reduced the ERK1/2 phosphorylation extent in HUVEC cells in a time-dependent manner (Figure 3A). No differences in ERK1/2 phosphorylation were observed in HUVEC cells after a scramble peptide administration (data not shown). Instead, cell growth assessment performed 24, 48, and 72 h after treatment showed a different behavior in HUVEC compared to HeLa cells. In fact, no significant differences were noticed 24 h after treatment compared to the control, while a 48% inhibition was reported with HeLa cells. Moreover, we only observed a 28% and 32% of cell growth inhibition 48 and 72 h after treatment, respectively (Figure 3B) versus 62.5% and 66.5% described 48 and 72 h after treatment of HeLa cells, respectively (see Table 1). To investigate the role of VEGFR2 on PTPRJ-pep19.4-mediated ERK1/2 dephosphorylation and cell growth inhibition on HUVECs, we assayed the phosphorylation state of VEGFR2 in VEGF-stimulated HUVECs treated with or without PTPRJ-pep19.4. As reported in Figure 3C, we observed a significant reduction of phospho-VEGFR2, thus suggesting an impaired signaling by this receptor in cells treated with PTPRJ-pep19.4.

The production of tubular structures is an important step in angiogenesis; therefore, as PTPRJ activity antagonizes VEGFR2 function,[21] we investigated the role of PTPRJ-pep19.4 on HUVEC tube formation. As shown in Figure 3D, control HUVEC cells, plated on Matrigel and incubated either with control medium or a scramble peptide, formed lumen-like structures, while HUVEC cells treated with PTPRJ-pep19.4 formed fewer tubes as well as fewer and weaker anastomoses.

PTPRJ-pep19.4 Negatively Modulates ERK1/2 Phosphorylation and Reduces Cell Proliferation of Mammary Cancer Cells. To evaluate if the effects of PTPRJ-pep19.4 on HeLa cells could be considered a general event in cancer cells, we also included in our investigation two mammary cancer cell lines,

dx.doi.org/10.1021/cb3007192 | ACS Chem. Biol. 2013, 8, 1497−1506

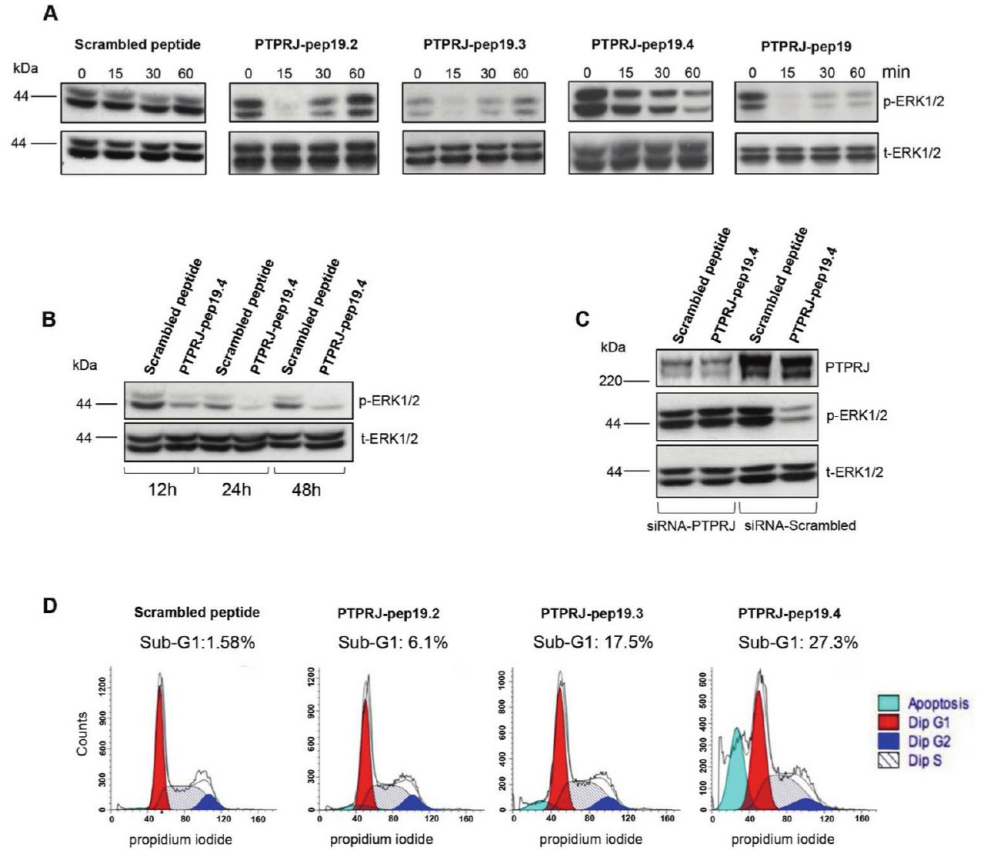

Figure 2. PTPRJ-pep19.2−4 synthetic peptides suppress phosphorylation of ERK1/2 and induce cell death of HeLa cancer cells. (A) HeLa cells were seeded in 6-well plates and, 24 h later, treated with 160 μM PTPRJ-pep19.2, PTPRJ-pep19.3, PTPRJ-pep19.4, native PTPRJ-pep19, or scrambled peptide at 0, 15, 30, and 60 min. Cell lysates were subjected to immunoblotting using a phospho-specific ERK1/2 (p-ERK) antibody. Blots were stripped and reprobed for total ERK1/2 as a loading control. (B) HeLa cells were treated either with 160 μM PTPRJ-pep19.4 or scrambled peptide, and cells were collected at the indicated intervals (12, 24, and 48 h). Cell lysates were subjected to immunoblots using phospho-specific ERK1/2 (p-ERK). Blots were stripped and reprobed for total ERK1/2 antibody as a loading control. (C) HeLa cells were transfected with either 100 nM PTPRJ or scrambled siRNAs and 48 h later were treated with either 160 μM PTPRJ-pep19.4 or scrambled peptide for 1 h. Cell lysates were subjected to immunoblotting using an anti-PTPRJ antibody and a phospho-specific ERK1/2 (p-ERK) antibody. Blots were stripped and reprobed for total ERK1/2 as a loading control.(D) Representative experiment of cell cycle analysis of HeLa cells treated with PTPRJ-pep19.2−4 synthetic peptides. The percentage of sub-G1 population is reported on the top of each histogram. Data analysis was performed with ModFit LTTM cell cycle analysis software.

MCF-7 and SKBr3, which both express endogenous PTPRJ (data not shown). Both cell lines were treated with 160 μM PTPRJ-pep19.4, as previously described, and both ERK1/2 phosphorylation and growth rate were assessed. PTPRJ-pep19.4 negatively modulated ERK1/2 phosphorylation extent in the short term (Figure 4A); moreover, we observed a significant cell growth inhibition resulting in a reduction of about 40% compared to controls in both cell lines (Figure 4C) at 72 h.

To check if PTPRJ-pep19.4 administration was toxic to normal cells, the above-described experiments were also carried out on primary human mammary epithelial cells (HMECs). Intriguingly, no effects on both ERK1/2 phosphorylation and proliferation were observed in normal cells (Figure 4B,C).

Molecular Modeling of Ala-scan PTPRJ-Binding Derivatives Suggests Supramolecular Aggregation States. Monte Carlo (MC) conformational search, docking experiments, thermodynamics, and statistical analyses were performed with the aim to rationalize at molecular level the biological properties of our PTPRJ agonist peptides comparing their structural features to those of the lead compound PTPRJ-pep19 (see Methods for further details).

As in the case of other PTPRJ peptide binders,[23] the MC search of PTPRJ-pep19.1 to -pep19.8 revealed a large number of local minimum energy conformers (Table 2).

This information was also confirmed by Boltzman population and clustering analyses. The graphical inspection of global minimum energy conformations, carried out by α carbons guided alignment of the new derivatives onto PTPRJ-pep19, showed a good superimposition to the lead compound (see Figure S3 in Supporting Information).

Following the same computational approach reported in our recent communication,[23] the self-aggregation trend of the new peptides was investigated by means of docking simulation coupled to thermodynamics and statistical analyses (see Methods). Results clearly indicate that all peptides formed multiple conformation self-aggregates with 1:1 stoichiometry (Table 3).

PTPRJ-pep19.1 to -pep19.3 and PTPRJ-pep19.5 to -pep19.8 reported an overall complexes stabilization (ΔG) notably weaker than that of PTPRJ-pep19. Only PTPRJ-pep19.4 maintained a thermodynamic profile comparable to the lead compound. Statistic data, obtained by coupling Boltzmann population and clustering analyses, revealed for all new derivatives, excluding PTPRJ-pep19.3, a number of possible geometry clusters larger than PTPRJ-pep19 and, with the exception of PTPRJ-pep19.1, increased population of the global minimum energy structures. Graphic inspection of the most stable complexes and their α carbons alignment onto PTPRJ-pep19 strongly indicated that

dx.doi.org/10.1021/cb3007192 | ACS Chem. Biol. 2013, 8, 1497−1506

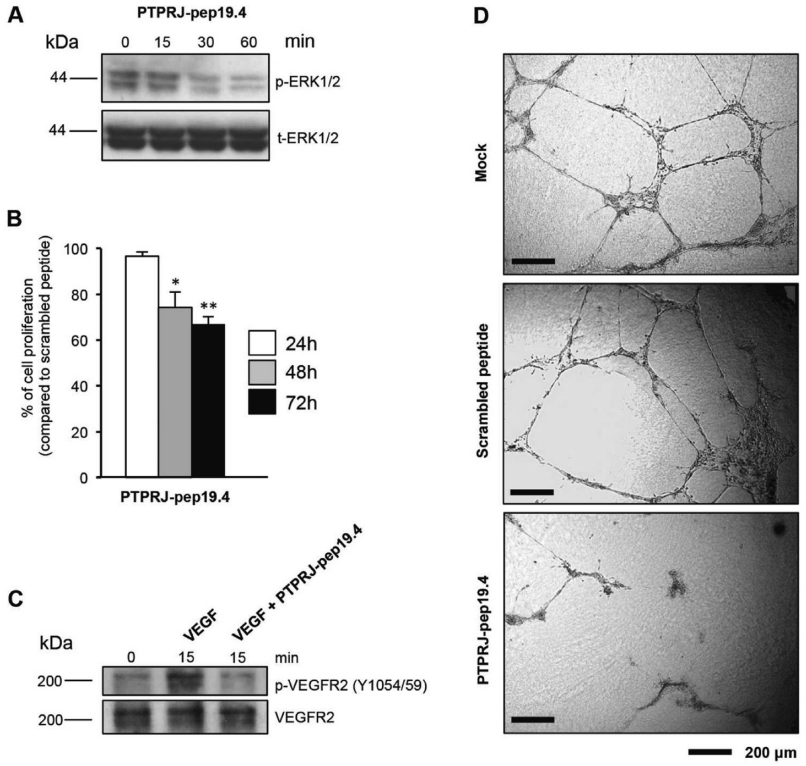

Figure 3. PTPRJ-pep19.4 negatively modulates ERK1/2 phosphorylation and inhibits both cell proliferation and tube formation of HUVEC endothelial cells. (A) PTPRJ-pep19.4 suppresses phosphorylation of ERK1/2 in HUVECs; cells were treated with 160 μM PTPRJ-pep19.4 and collected at the indicated intervals (15−60 min). Cell lysates were subjected to immunoblots using phospho-specific ERK1/2 (p-ERK). Blots were stripped and reprobed for total ERK1/2 antibody as a loading control. (B) Cell growth inhibition induced by PTPRJ-pep19.4 in HUVECs at 24 h (white columns), treated every 24 h for 48 h (gray columns) and every 24 h for 72 h (black column). Results represent the mean ± SD of three independent experiments. $^*P < 0.05$, $^{**}P < 0.01$ compared to scrambled peptide by unpaired two-tailed Student's t test. (C) HUVECs were serum starved, stimulated with 20 ng/mL of VEGF, treated 15 min with or without PTPRJ-pep19.4, and then lysed. VEGFR2 phosphorylation levels were detected by immunoblotting with a phospho-specific VEGFR2 (Y1054/1059) antibody. Membranes were stripped and immunoblotted with a VEGFR2 antibody. (D) PTPRJ-pep19.4 inhibits tube formation of primary endothelial cells on Matrigel. Representative photograph of antitube formation activity of PTPRJ-pep19.4. HUVECs (2.5×10^4/well) were untreated or preincubated either with PTPRJ-pep19.4 or scrambled peptide (100 μM) for 30 min before being seeded onto the solidified Matrigel for 18 h. (scale bar: 200 μM).

Table 2. Monte Carlo Conformational Search and Clustering Results of PTPRJ-pep19 to -pep19.8 Peptides[a]

							lowest energy cluster		
PTPRJ peptides	*n*Tor	TNC	av	NPC	GMP	clusters	Boltzman population (%)	cluster members	RMSd
19[b]	32	36909	1.03	69	25.34	5478	29.09	7	0.00
19.1	30	14782	1.26	90	7.58	1566	60.63	76	2.67
19.2	29	51751	1.33	103	8.92	6907	50.26	63	3.20
19.3	29	21153	1.97	32	37.83	1411	94.87	384	2.49
19. 4	31	53356	1.61	146	13.20	5020	45.40	1189	0.18
19.5	29	30073	2.17	72	25.38	3654	66.12	639	0.16
19.6	29	27616	1.80	106	3.49	4297	3.92	26	3.73
19.7	29	27606	2.31	74	28.61	1570	90.97	3532	0.96
19.8	30	13452	1.30	94	22.87	1113	59.44	201	2.80

[a] *n*Tor = rotatable bonds taken into account for MC search; TNC = MC generated conformers; av = average number of duplicate structures; NPC = number of conformers with a Boltzman population ≥ 0.1%; GMP = Boltzman population of the global minimum energy conformer in percentage. RMSd = α carbons root-mean-square deviation (in Å) between the global minimum energy conformer with respect to PTPRJ-pep19. [b] Previously published data.

only PTPRJ-pep19.4 could be related to the lead compound (Figure 5), while all other derivatives were different in terms of both shape and chemical features exposition (Figure S4 in Supporting Information).

NMR Analysis Indicates That PTPRJ-pep19.4 Folds as a β-Turn and Shows Propensity to Dimerization. The most promising peptide PTPRJ-pep19.4 was also investigated by solution NMR in water solution. Similarly to its precursor PTPRJ-pep19,[23] the spectra showed splitting of the signals. Complete ^{1}H NMR chemical shift assignments (Table S1 in Supporting Information) were achieved for the most intense signal pattern according to the Wüthrich procedure.[24] NMR parameters of the peptide indicated high conformation flexibility illustrated, for example, by the absence of medium range

dx.doi.org/10.1021/cb3007192 | ACS Chem. Biol. 2013, 8, 1497−1506

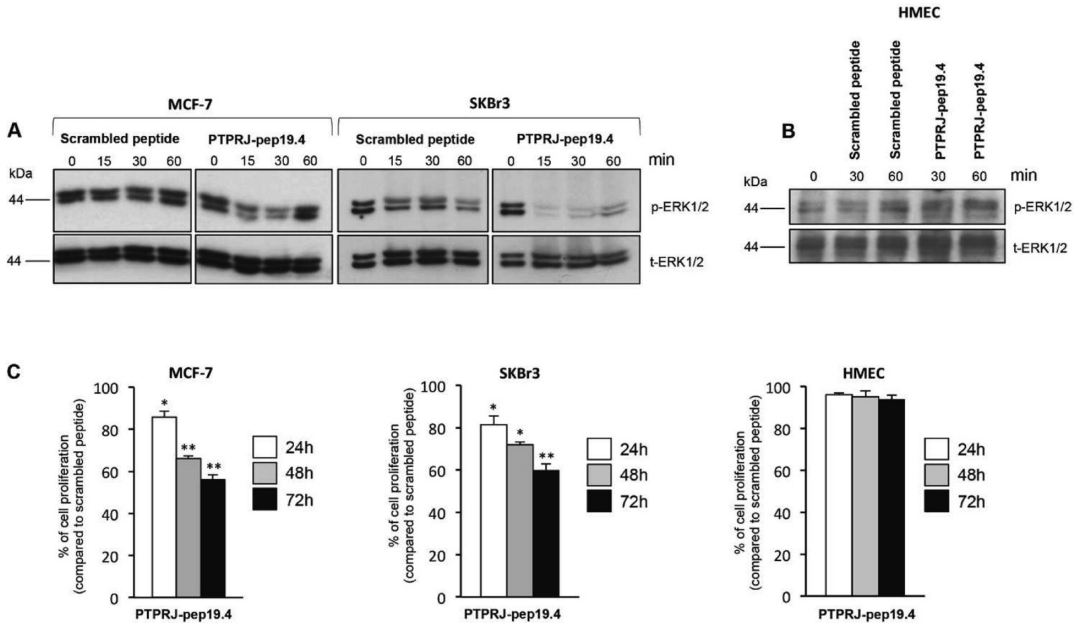

Figure 4. PTPRJ-pep19.4 negatively modulates ERK1/2 phosphorylation and reduces cell proliferation of human mammary cancer cells. (A) MCF-7 and SKBr3 cells were seeded in 6-well plates and,24 h later, treated with either 160 μM PTPRJ-pep19.4 or scrambled peptide, and lysed at 0, 15, 30, 60 min. Cell lysates were subjected to immunoblotting using a phospho-specific ERK1/2 (p-ERK) antibody. Blots were stripped and reprobed for total ERK1/2 as a loading control. B) HMECs were treated with 160 μM PTPRJ-pep19.4 or scrambled peptide, and cells were collected at the indicated intervals. Cell lysates were subjected to immunoblots using phospho-specific ERK1/2 (p-ERK). Blots were stripped and reprobed for total ERK1/2 antibody as a loading control. (C) Cell growth rate of MCF7, SKBr3, and HMECs by PTPRJ-pep19.4 peptide. Relative cell growth (as a percentage of the growth observed in cells treated with scrambled peptide) at different intervals of treatments (from 24 to 72 h) is reported. Cells were treated once with PTPRJ-pep19.4 and scrambled peptides for 24 h (white columns) or treated every 24 h for 48 h (gray columns) and for 72 h (black columns). Results represent the mean ± SD of three independent experiments. *$P < 0.05$, **$P < 0.01$ compared to scrambled peptide by unpaired two-tailed Student's t test.

Table 3. Theoretical Investigation of Aggregation Processes of PTPRJ-pep19 to -pep19.8[a]

		docking		energy minimized					
PTPRJ peptides	DC	10 kcal/mol	3 kcal/mol	all optimized structures	global min energy structure population	ΔG (kcal/mol)	ΔH (kcal/mol)	ΔS (cal/mol)	RMSd
19[b]	67	3996612	76990	1014	18.80	−33.5	−31.7	6.19	0.00
19.1	90	7597571	170597	106092	2.05	−28.0	−25.9	7.16	5.87
19.2	103	10402442	174397	106453	20.52	−24.4	−23.4	3.40	2.95
19.3	32	1004962	15916	9513	26.94	−19.3	−17.8	4.97	5.04
19.4	146	20037354	332051	204911	85.37	−32.8	−32.3	1.44	1.36
19.5	72	4691090	52357	27320	83.76	−23.8	−23.5	0.98	6.00
19.6	106	12190758	191948	139403	22.74	−22.5	−20.5	6.45	5.27
19.7	74	5566721	84610	55456	79.73	−28.7	−28.0	2.31	5.79
19.8	94	8597500	111469	64761	55.36	−26.4	−25.5	2.93	6.28

[a]DC = host/guest docked conformations; docking = complexes within 10 and 3 kcal/mol; RMSd = α carbons root-mean-square deviation (in Å) between the global minimum energy conformer with respect to PTPRJ-pep19.[b] [b]Previously published data.

diagnostic NOEs apart from a weak signal between Hβs of ^{4}Ala and HN of ^{6}Thr. This signal indicates that a β-turn structure centered on residues ^{4}Ala-^{5}Leu is present in a population of conformers. Upfield shift of HN signals of residues ^{5}Leu and ^{6}Thr, compared to the corresponding in PTPRJ-pep19[23] and relatively low temperature coefficient of HN-6 ($-\Delta\delta/\Delta T = 4.3$ ppb/K, Table S1 in Supporting Information), confirms this hypothesis being indicative of the presence of H-bonds involving these amide protons. Unfortunately, diagnostic Hα-HN i,i+2 NOE signal between residues 4 and 6 could not be observed due to overlapping. This turn structure is in accordance with the molecular modeling results (Figure 5). Furthermore, to check the aggregation state of PTPRJ-pep19.4 under the NMR conditions, STD-NMR experiments[25] were recorded (Figure S5 in Supporting Information). As for PTPRJ-pep19, on-resonance irradiation induces detectable STD signals with relative STD effect of about 1% (0.7% was found for PTPRJ-pep19), suggesting that aggregation properties of the two peptides are similar with high propensity to dimerization.[23]

Conclusions. As recently reviewed,[26] protein phosphatases represent a very interesting target for the development of novel therapeutics. The ability of PTPRJ to counteract the signaling from several protein kinases either transmembrane or soluble involved in the aberrant mitogenic signals[16−19,21,27] makes this protein tyrosine phosphatase receptor a particularly intriguing target for the generation of a novel class of protein kinase inhibitors as anticancer drugs in addition to monoclonal antibodies and small molecules already available for current cancer therapies.[3]

dx.doi.org/10.1021/cb3007192 | ACS Chem. Biol. 2013, 8, 1497−1506

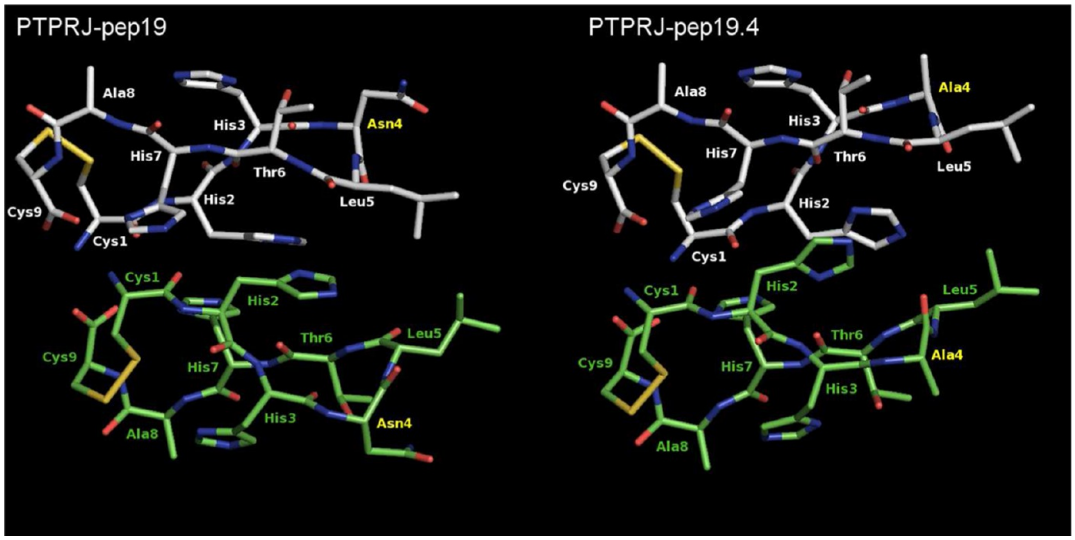

Figure 5. Graphic comparison of PTPRJ-pep19 and PTPRJ-pep19.4 most stable self-aggregates. Peptides are depicted in polytube, and complex subunits are colored in CPK and green carbons, respectively.

It is easily arguable that PTPRJ signaling follows the interaction between a ligand and its ectodomain. However, for a long time after its discovery, PTPRJ remained an orphan receptor. The first clue about a PTPRJ biological ligand came from Sörby and colleagues,[28] who demonstrated that some unspecified components of Matrigel could trigger PTPRJ signaling. Only recently, two large molecules have been discovered as PTPRJ ligands, syndecan-2 and TSP-1.[29,30] However, although important in the understanding of PTPRJ physiology, these molecules are very far from being conceived as therapeutic agents to be used for PTPRJ stimulation either in cancer or endothelial cells with the purpose to inhibit both tumor growth and angiogenesis, two hallmarks of cancer.[20] The first experimentally successful attempt to stimulate PTPRJ in a "therapeutic" way was done by Takahashi and colleagues,[22] who proved that the administration of a monoclonal antibody raised against PTPRJ was able to inhibit *in vivo* angiogenesis. An intriguing way to generate PTPRJ agonists was recently pursued by our group;[23] in fact, through a screening of a combinatorial phage display library, we identified two peptides (PTPRJ-pep19 and -pep24) able to bind and trigger PTPRJ activity in both cancer and endothelial cells. Their stimulation resulted in the reduction of MAPK phosphorylation and slight inhibition of cell proliferation; also, a weak percentage of apoptosis was assessed.

With the aim to derive structure−activity relationship, we have begun a study to address the contribution of the various amino acids residues of PTPRJ-pep19 through an Ala-scan analysis. This approach would also eventually allow us to select other compounds with an improved biological activity on both cancer and endothelial cells. Therefore, starting from PTPRJ-pep19, we generated a panel of peptides to be tested on HeLa and HUVEC cells. Our results suggest that cyclic structure is strongly required for the biological activity of effective peptides, as linear peptides basically showed no activity even if primary structure corresponded to PTPRJ-pep19. The substitution in the lead compound of ^{4}Asn with Ala led to derivative PTPRJ-pep19.4 with a strongly improved antiproliferative activity. In fact, PTPRJ-pep19.4 showed a great ability in inhibiting HeLa cell growth (66% compared to 20% of the native PTPRJ-pep19 sequence). Cell growth inhibition was also observed in HUVECs, although the effect was significantly lower than in HeLa cells, suggesting a good profile of "cell selectivity" of our compound, especially at 24 h. Intriguingly, while both ERK1/2 phosphorylation and cell proliferation were inhibited in mammary cancer cells treated with PTPRJ-pep19.4, no effects were observed in primary mammary cells, indicating lack of toxicity of PTPRJ-pep19.4 in normal cells.

As described with PTPRJ-pep19, PTPRJ-pep19.4 was also able to reduce the phosphorylation extent of MAPK in both HeLa and HUVEC cells; however, the pattern of dephosphorylation was quite different. In fact, while MAPK dephosphorylation reached its highest degree in the short term within 15 min after stimulation with PTPRJ-pep19 and its partly effective derivatives (PTPRJ-pep19.2 and -pep19.3), PTPRJ-pep19.4 resulted in a time-dependent MAPK dephosphorylation, reaching its highest peak 60 min after its administration. We might speculate that this effect could be dependent on the higher stability of the binding between PTPRJ-pep19.4 and PTPRJ ectodomain compared to the other peptides (i.e., PTPRJ-pep19.2/3), which might be able to transduce a more persistent signal into treated cells. However, even though the effects of PTPRJ-pep19.4 on cell proliferation were similar in all cancer cell lines investigated in this study, the time course of MAPK dephosphorylation in mammary SKBr3 cells was different if compared to HeLa and MCF-7 cells suggesting that such different behavior of MAPK dephosphorylation might be cell-type-dependent.

As TSP-1, a natural ligand of PTPRJ,[30] is a natural inhibitor of the sprouting of new blood vessels from preexisting ones,[31] we checked if *in vitro* inhibition of angiogenesis could also be evoked by our synthetic PTPRJ-pep19.4 peptide. Importantly, PTPRJ-pep19.4 showed ability in blocking the organization of HUVECs into tubular structures in Matrigel; this finding further supports the idea that PTPRJ-pep19.4 could be a useful tool in the design and discovery of additional agents that can inhibit pathologic neovascularization. Our data are coherent with results proposed by Brunner and colleagues,[32] who demonstrated that *PTPRJ*-overexpression in HUVECs was able to effectively inhibit tube formation, even though, more recently, Spring et al. proposed that PTPRJ has an opposite effect on the *in vitro* formation of branched capillary-like structures.[33]

Molecular modeling results and NMR data revealed, similarly to the already reported peptides,[23] a large conformational space

dx.doi.org/10.1021/cb3007192 | *ACS Chem. Biol.* 2013, 8, 1497−1506

for all new derivatives and their tendency to self-aggregate, even if the new compound complexes showed a theoretical energy stabilization lower than that of the precursor. Due to the unavailability of a 3D model of the target, the role of the omodimerization cannot be completely clarified, but it is reasonable to expect its involvement in the peptide-receptor recognition, as previously suggested.[22,34]

In conclusion, our study represents a significant advancement in the structure−activity relationship knowledge related to the presented class of PTPRJ agonist peptides; moreover, our findings strongly encourage the applications of further chemical modifications to PTPRJ peptides with the aim to create a novel class of small molecules with improved biological activity with the final goal to translate them into clinical practice.

METHODS

Synthesis of Ala-scan PTPRJ Derivatives. The synthesis of PTPRJ analogues was performed according to the solid phase approach using standard Fmoc methodology in a manual reaction vessel.[35] N^{α}-Fmoc-protected amino acids, Wang-resin, HOBt, HBTU, DIEA, piperidine, and trifluoroacetic acid were purchased from Iris Biotech (Germany). Peptide synthesis solvents, reagents, and CH_3CN for HPLC were reagent grade and were acquired from commercial sources and used without further purification unless otherwise noted. The first amino acid, N^{α}-Fmoc-Cys(Trt)-OH was coupled to Wang resin (0.2 g, 0.7 mmol of NH_2/g). The following protected amino acids were then added stepwise: N^{α}-Fmoc-Ala-OH, N^{α}-Fmoc-His($N_{(im)}$-trityl (trt))-OH, N^{α}-Fmoc-Thr(*O-tert*-butyl (tBu))-OH, N^{α}-Fmoc-Leu-OH, N^{α}-Fmoc-Asn (N_{γ}-trityl, trt)-OH, N^{α}-Fmoc-Cys(trt)-OH. Each coupling reaction was accomplished using a 3-fold excess of amino acid with HBTU and HOBt in the presence of DIEA (6 equiv). The N^{α}-Fmoc protecting groups was removed by treating the protected peptide resin with a 25% solution of piperidine in DMF (1 × 5 min and 1 ×x 25 min). The peptide resin was washed three times with DMF, and the next coupling step was initiated in a stepwise manner. The peptide resin was washed with DCM (3×), DMF (3×), and DCM (3×), and the deprotection protocol was repeated after each coupling step.

The N-terminal Fmoc group was removed as described above, and the peptide was released from the resin with TFA/iPr_3SiH/H_2O (90:5:5) for 3 h. The resin was removed by filtration, and the crude peptide was recovered by precipitation with cold anhydrous ethyl ether to give a white powder and then lyophilized.

General Method of Disulfide Bridge Formation. Air oxidation was carried out by dissolving 50 mg of the lyophilized crude peptide in 90 mL of 1:1 0.1 M NH_4HCO_3/isopropyl alcohol (pH 8.25) with vigorous stirring at RT for 1 h. Prior to purification, the solution was acidified to pH 3 with TFA and analyzed by analytical HPLC. The solution was concentrated using a rotary evaporator at 30 °C and then lyophilized.[36]

Purification and Characterization of Ala-scan PTPRJ Derivatives. All crude cyclic peptides were purified by RP-HPLC on a semipreparative C18-bonded silica column (Phenomenex, Jupiter, 250 mm × 10 mm) using a Shimadzu SPD 10A UV−vis detector, with detection at 210 nm and 254 nm. The column was perfused at a flow rate of 3 mL/min with solvent A (10%, v/v, water in 0.1% aqueous TFA), and a linear gradient from 10% to 90% of solvent B (80%, v/v, acetonitrile in 0.1% aqueous TFA) over 40 min was adopted for peptide elution. Analytical purity and retention time (t_R) of each peptide were determined using HPLC conditions in the above solvent system (solvents A and B) programmed at a flow rate of 1 mL/min using a linear gradient from 10% to 90% B over 25 min, fitted with C-18 column Phenomenex, Juppiter C-18 column (250 mm × 4.60 mm; 5 μm). All analogues showed >97% purity when monitored at 215 nm. Homogeneous fractions, as established using analytical HPLC, were pooled and lyophilized.

Peptides molecular weights were determined by ESI mass spectrometry. ESI-MS analysis in positive ion mode, were made using a Finnigan LCQ Deca ion trap instrument, manufactured by Thermo Finnigan (San Jose, CA, USA), equipped with the Excalibur software for processing the data acquired. The sample was dissolved in a mixture of water and methanol (50/50) and injected directly into the electrospray source, using a syringe pump, which maintains constant flow at 5 μL/min. The temperature of the capillary was set at 220 °C.

Cell Lines and Transfections. HeLa cervical cancer cells and MCF-7 and SKBr3 mammary cancer cells were purchased from the American Type Culture Collection (ATCC). Cells were cultured in RPMI medium 1640 supplemented with 10% heat-inactivated FBS (Invitrogen). Human umbilical vein endothelial cells (HUVEC) (Clonetics) were cultured in M199 medium (Sigma-Aldrich) supplemented with 10% FBS, heparin (100 μg/mL; Sigma-Aldrich), and 10 ng/mL endothelial cell growth factor. Human mammary epithelial cells (HMECs) were purchased from Invitrogen and cultured as recommended by the manufacturer. Transfections were made with Lipofectamine 2000 (Invitrogen) by following the manufacturer's instructions; 4×10^5 cells were seeded in 6-well plates and transfected with 100 nM of either PTPRJ-specific and scrambled siRNAs, as previously described.[37] Human recombinant $VEGF_{165}$ was purchased from ORF Genetics.

Cell Survival Assay. To assess peptides-mediated inhibition of cell proliferation, HeLa and HUVECs were treated once with peptides for 24 h or treated every 24 h for 48 h and every 24 h for 72 h at the concentration of 160 μM. At the end of treatments, cells were trypsinized and counted, and cell viability was determined by the trypan blue dye exclusion test. The results were expressed as percent variation in the number of viable cells treated with PTPRJ-peptides compared with control peptide treated cells.

Antibodies and Western Blot Analysis. ERK1/2, VEGFR2, and phospho-ERK1/2 antibodies were purchased from Santa Cruz Biotechnology (Santa Cruz, CA). Phospho-VEGFR2 Y1054/59 was purchased by Invitrogen. Horseradish peroxidase (HRP)-conjugated anti-goat and anti-rabbit immunoglobulins were also from Santa Cruz Biotechnology. Cells were scraped in ice-cold phosphatase-buffered saline (PBS) and lysed in NP-40 lysis buffer containing 50 mM Tris-HCl, pH 7.5, 150 mM NaCl, 1% NP-40, one protease inhibitor mixture tablet per 10 mL of buffer (Completet, Roche Diagnostics), 1 mM Na_3VO_4, and 50 mM NaF. Lysates were passed several times through a 21-gauge needle and incubated for 30 min on ice. Cellular debris was pelleted by centrifugation at 10,000*g* for 15 min at 4 °C. Protein concentrations were determined using the Bradford protein assay dye (Bio-Rad Laboratories, Hercules, CA). Total cell lysates were separated by SDS−PAGE and transferred to PVDF membranes. Membranes were blocked in 5% nonfat dry milk (Bio-Rad) and then probed for about 2 h with primary antibodies. After incubation with specific (HRP)-conjugated secondary antibodies, protein bands were revealed by the ECL detection system (Santa Cruz Biotechnology).

Cell Cycle Distribution Analysis. The cells were plated at 0.5×10^6 cells/60 mm dish and sequential treated every 24 h for 72 h with 160 μM peptides (Invitrogen, Carlsbad, CA). Cells were harvested and fixed with cold 70% ethanol. Before analysis, cells were washed with PBS and stained with a solution containing 50 μg/mL propidium iodide, 250 μg/mL RNAase, and 0.04% Nonidet P40 (NP40) for 30 min at RT in the dark. The fluorescence of stained cells was analyzed by flow cytometry using a FACSCanto (Becton Dickinson). A flow cytometric sub-G1 peak was detected on DNA plots using ModFit LT cell cycle analysis software (Verity software House).

Endothelial Cell Tube Formation Assay. Unpolymerized Matrigel (Becton Dickinson, Mountain View, CA) was placed (50 μL per well) in a 96-well microtiter plate (0.32 cm^2 per well) and polymerized for 1 h at 37 °C. HUVECs (2.5×10^4 well) were preincubated with PTPRJ-pep19.4 or scrambled peptide (100 μM) for 30 min before being seeded onto the solidified Matrigel. After incubating in media for 18 h, cells were fixed, and tube formation was analyzed by light microscopy (Leica, Germany). Two random fields were chosen in each well.

NMR Spectroscopy. Samples for NMR spectroscopy were prepared by dissolving the appropriate amount of peptide in 0.55 mL of ^1H_2O and 0.05 mL of ^2H_2O or 0.60 mL of ^2H_2O containing phosphate-buffered saline (50 mM) at pH 4.0 and 5 °C. NMR spectra were recorded on a Varian INOVA 700 MHz spectrometer equipped with a *z*-gradient

5 mm triple-resonance probe head. Spectra were calibrated relative to TSP (0.00 ppm) as internal standard. One-dimensional (1D) NMR spectra were recorded in the Fourier mode with quadrature detection. Water suppression was achieved by using the double-pulsed field gradient spin−echo (DPFGSE) scheme.[38] 2D TOCSY[39] and NOESY[40] spectra were recorded in the phase-sensitive mode using the method from States et al.[41] Data block sizes were 2048 addresses in t_2 and 512 equidistant t_1 values. Before Fourier transformation, the time domain data matrices were multiplied by shifted $\sin^2$ functions in both dimensions. A mixing time of 70 ms was used for the TOCSY experiments. NOESY experiments were run with mixing time of 200−600 ms. The quantitative analysis of NOESY spectra was obtained using the interactive program package XEASY.[42] The temperature coefficients of the amide proton chemical shifts were calculated from TOCSY experiments performed at different temperatures in the range 5−15 °C by means of linear regression. STD-NMR (25) experiments were performed in ^2H_2O solution with on-resonance and off-resonance saturation at $\delta = -2$ and -16 ppm, respectively. Typically, 512 scans were recorded for each STD spectrum (saturation time = 2 s). The relative STD effect (STD%) was calculated as the ratio between the intensity (expressed as S/N ratio) of the signals in the STD spectrum and that of the signals in the ^{1}H NMR spectrum.

Molecular Modeling. 3D theoretical models of all peptides were built by means of L series residues using ver. 9.1 of the Maestro GUI.[43] Using the Monte Carlo (MC) search, implemented in MacroModel ver. 9.8[43,44] for each compound, by randomly rotate all possible dihedral angles, one million of conformations were generated. Each MC structure was optimized using 10000 steps of the Polak Ribiere Conjugate Gradient algorithm and energy evaluated with the all atoms notation of AMBER* force field.[45] Water solvent effects were mimicked according to the GB/SA implicit model.[46] Conformers with similar internal energies, within 4.184 kJ/mol, were geometrically compared one each other by computing the root-mean-square deviation (RMSd) onto their not hydrogen atoms and were considered duplicate if the RMSd value was lower than 0.05 Å. Boltzman population analysis was performed, at 300° K, onto all MC sampled structures reporting internal energy within 50 kJ/mol from the global minimum. MC ensembles were submitted to cluster analysis using an RMSd cutoff distance equal to 0.5 Å, computed onto the non-hydrogen atoms.[47] Boltzman population data were considered for weighting the cluster analysis results. Aggregation processes were investigated using our *in house* docking software MolInE[48,49] that automatically generated bimolecular complexes. Each MC conformer with a Boltzman population larger than 0.1% was considered as both host and guest. According to MolInE methodology, the autorecognition of our peptides was systematically explored by rigid body roto-translation of the guest, with respect to the host. Docking configurations were energy evaluated using the all atoms notation of the AMBER* force field.[41] Water environment was mimicked by defining the dielectric constant equal to 80. The MolInE grid resolution (GR) and van der Waals compression factor (x) were fixed to 6 and 0.6, respectively. The same force field, environment, and deduplication criterion, previously described for the MC search, were adopted for taking into account induced fit phenomena and to discard equivalent structures. The thermodynamics module of MolInE was used to evaluate the stability of the complexes calculating the corresponding binding energies.

Statistical Methods and Data Analysis. All experiments were performed in triplicate from at least three independent experiments, and data shown are the means ± standard deviation (SD). When only two groups were compared, statistical differences were assessed with unpaired two-tailed Student's *t* test. Statistical analyses were performed using GraphPad Prism 5 software. For all analyses, differences were considered significant if $P < 0.05$.

■ ASSOCIATED CONTENT

Ⓢ Supporting Information

This material is available free of charge *via* the Internet at http://pubs.acs.org.

■ AUTHOR INFORMATION

Corresponding Author

*E-mail: pcampigl@unisa.it; trapasso@unicz.it.

Author Contributions

#These authors contributed equally to this work.

Notes

The authors declare no competing financial interest.

■ ACKNOWLEDGMENTS

The present study was supported by a grant from the Associazione Italiana Ricerca Cancro (AIRC). This study was also partly supported by the Fondazione Università Magna Græcia. This paper is dedicated to the memory of C. Stillitani, brilliant student and wonderful person, who decided to stay forever in Catanzaro, the place he loved.

■ REFERENCES

(1) Blume-Jensen, P., and Hunter, T. (2001) Oncogenic kinase signalling. *Nature 411*, 355−365.

(2) Sawyers, C. (2004) Targeted cancer therapy. *Nature 432*, 294−297.

(3) Zhang, J., Yang, P. L., and Gray, N. S. (2009) Targeting cancer with small molecule kinase inhibitors. *Nat. Rev. Cancer 9*, 28−39.

(4) Easty, D., Gallagher, W., and Bennett, D. C. (2006) Protein tyrosine phosphatases, new targets for cancer therapy. *Curr. Cancer Drug Targets 6*, 519−532.

(5) Honda, H., Inazawa, J., Nishida, J., Yazaki, Y., and Hirai, H. (1994) Molecular cloning, characterization, and chromosomal localization of a novel protein-tyrosine phosphatase, HPTPeta. *Blood 84*, 4186−4194.

(6) Ostman, A., Yang, Q., and Tonks, N. K. (1994) Expression of DEP-1, a receptor-like protein-tyrosine-phosphatase, is enhanced with increasing cell density. *Proc. Natl. Acad. Sci. U.S.A. 91*, 9680−9684.

(7) Ostman, A., Hellberg, C., and Bohmer, F. D. (2006) Protein-tyrosine phosphatases and cancer. *Nat. Rev. Cancer 6*, 307−320.

(8) Trapasso, F., Drusco, A., Costinean, S., Alder, H., Aqeilan, R. I., Iuliano, R., Gaudio, E., Raso, C., Zanesi, N., Croce, C. M., and Fusco, A. (2006) Genetic ablation of Ptprj, a mouse cancer susceptibility gene, results in normal growth and development and does not predispose to spontaneous tumorigenesis. *DNA Cell Biol. 25*, 376−382.

(9) Iuliano, R., Le Pera, I., Cristofaro, C., Baudi, F., Arturi, F., Pallante, P., Martelli, M. L., Trapasso, F., Chiariotti, L., and Fusco, A. (2004) The tyrosine phosphatase PTPRJ/DEP-1 genotype affects thyroid carcinogenesis. *Oncogene 23*, 8432−8438.

(10) Zhang, L., Martelli, M. L., Battaglia, C., Trapasso, F., Tramontano, D., Viglietto, G., Porcellini, A., Santoro, M., and Fusco, A. (1997) Thyroid cell transformation inhibits the expression of a novel rat protein tyrosine phosphatase. *Exp. Cell Res. 235*, 62−70.

(11) Trapasso, F., Iuliano, R., Boccia, A., Stella, A., Visconti, R., Bruni, P., Baldassarre, G., Santoro, M., Viglietto, G., and Fusco, A. (2000) Rat protein tyrosine phosphatase eta suppresses the neoplastic phenotype of retrovirally transformed thyroid cells through the stabilization of p27(Kip1). *Mol. Cell. Biol. 20*, 9236−9246.

(12) Ruivenkamp, C. A., van Wezel, T., Zanon, C., Stassen, A. P., Vlcek, C., Csikós, T., Klous, A. M., Tripodis, N., Perrakis, A., Boerrigter, L., Groot, P. C., Lindeman, J., Mooi, W. J., Meijjer, G. A., Scholten, G., Dauwerse, H., Paces, V., van Zandwijk, N., van Ommen, G. J., and Demant, P. (2002) Ptprj is a candidate for the mouse colon-cancer susceptibility locus Scc1 and is frequently deleted in human cancers. *Nat. Genet. 31*, 295−300.

(13) Ruivenkamp, C., Hermsen, M., Postma, C., Klous, A., Baak, J., Meijer, G., and Demant, P. (2003) LOH of PTPRJ occurs early in colorectal cancer and is associated with chromosomal loss of 18q12-21. *Oncogene 22*, 3472−3474.

(14) Iuliano, R., Trapasso, F., Le Pera, I., Schepis, F., Samà, I., Clodomiro, A., Dumon, K. R., Santoro, M., Chiariotti, L., Viglietto, G., and Fusco, A. (2003) An adenovirus carrying the rat protein tyrosine

phosphatase eta suppresses the growth of human thyroid carcinoma cell lines in vitro and in vivo. *Cancer Res. 63*, 882−886.
(15) Trapasso, F., Yendamuri, S., Dumon, K. R., Iuliano, R., Cesari, R., Feig, B., Seto, R., Infante, L., Ishii, H., Vecchione, A., During, M. J., Croce, C. M., and Fusco, A. (2004) Restoration of receptor-type protein tyrosine phosphatase eta function inhibits human pancreatic carcinoma cell growth in vitro and in vivo. *Carcinogenesis 25*, 2107−2114.
(16) Kovalenko, M., Denner, K., Sandström, J., Persson, C., Gross, S., Jandt, E., Vilella, R., Böhmer, F., and Ostman, A. (2000) Site-selective dephosphorylation of the platelet-derived growth factor beta-receptor by the receptor-like protein-tyrosine phosphatase DEP-1. *J. Biol. Chem. 275*, 16219−16226.
(17) Palka, H. L., Park, M., and Tonks, N. K. (2003) Hepatocyte growth factor receptor tyrosine kinase met is a substrate of the receptor protein-tyrosine phosphatase DEP-1. *J. Biol. Chem. 278*, 5728−5735.
(18) Iervolino, A., Iuliano, R., Trapasso, F., Viglietto, G., Melillo, R. M., Carlomagno, F., Santoro, M., and Fusco, A. (2006) The receptor-type protein tyrosine phosphatase J antagonizes the biochemical and biological effects of RET-derived oncoproteins. *Cancer Res. 66*, 6280−6287.
(19) Berset, T. A., Hoier, E. F., and Hajnal, A. (2005) The C. elegans homolog of the mammalian tumor suppressor Dep-1/Scc1 inhibits EGFR signaling to regulate binary cell fate decisions. *Genes Dev. 19*, 1328−1340.
(20) Hanahan, D., and Weinberg, R. A. (2011) Hallmarks of cancer: the next generation. *Cell 144*, 646−674.
(21) Lampugnani, M. G., Zanetti, A., Corada, M., Takahashi, T., Balconi, G., Breviario, F., Orsenigo, F., Cattelino, A., Kemler, R., Daniel, T. O., and Dejana, E. (2003) Contact inhibition of VEGF-induced proliferation requires vascular endothelial cadherin, beta-catenin, and the phosphatase DEP-1/CD148. *J. Cell. Biol. 161*, 793−804.
(22) Takahashi, T., Takahashi, K., Mernaugh, R. L., Tsuboi, N., Liu, H., and Daniel, T. O. (2006) A monoclonal antibody against CD148, a receptor-like tyrosine phosphatase, inhibits endothelial-cell growth and angiogenesis. *Blood 108*, 1234−1242.
(23) Paduano, F., Ortuso, F., Campiglia, P., Raso, C., Iaccino, E., Gaspari, M., Gaudio, E., Mangone, G., Carotenuto, A., Bilotta, A., Narciso, D., Palmieri, C., Agosti, V., Artese, A., Gomez-Monterrey, I., Sala, M., Cuda, G., Iuliano, R., Perrotti, N., Scala, G., Viglietto, G., Alcaro, S., Croce, C. M., Novellino, E., Fusco, A., and Trapasso, F. (2012) Isolation and functional characterization of peptide agonists of PTPRJ, a tyrosine phosphatase receptor endowed with tumor suppressor activity. *ACS Chem. Biol. 7*, 1666−1676.
(24) Wüthrich, K. (1986) *NMR of Proteins and Nucleic Acids*; John Wiley & Sons, Inc., New York.
(25) Mayer, M., and Meyer, B. (1999) Characterization of ligand binding by saturation transfer difference NMR spectroscopy. *Angew. Chem., Int. Ed. 38*, 1784−1788.
(26) De Munter, S., Köhn, M., and Bollen, M. (2013) Challenges and opportunities in the development of protein phosphatase-directed therapeutics. *ACS Chem. Biol. 8*, 36−45.
(27) Sacco, F., Tinti, M., Palma, A., Ferrari, E., Nardozza, A. P., Hooft van Huijsduijnen, R., Takahashi, T., Castagnoli, L., and Cesareni, G. (2009) Tumor suppressor density-enhanced phosphatase-1 (DEP-1) inhibits the RAS pathway by direct dephosphorylation of ERK1/2 kinases. *J. Biol. Chem. 284*, 22048−22058.
(28) Sorby, M., Sandstrom, J., and Ostman, A. (2001) An extracellular ligand increases the specific activity of the receptor-like protein tyrosine phosphatase DEP-1. *Oncogene 20* (37), 5219−5224.
(29) Whiteford, J. R., Xian, X., Chaussade, C., Vanhaesebroeck, B., Nourshargh, S., and Couchman, J. R. (2011) Syndecan-2 is a novel ligand for the protein tyrosine phosphatase receptor CD148. *Mol. Biol. Cell 22*, 3609−3624.
(30) Takahashi, K., Mernaugh, R. L., Friedman, D. B., Weller, R., Tsuboi, N., Yamashita, H., Quaranta, V., and Takahashi, T. (2012) Thrombospondin-1 acts as a ligand for CD148 tyrosine phosphatase. *Proc. Natl. Acad. Sci. U.S.A. 109*, 1985−1990.
(31) Bouck, N., Stellmach, V., and Hsu, S. C. (1996) How tumors become angiogenic. *Adv. Cancer Res. 69*, 135−174.
(32) Brunner, P. M., Heier, P. C., Mihaly-Bison, J., Priglinger, U., Binder, B. R., and Prager, G. W. (2011) Density enhanced phosphatase-1 down-regulates urokinase receptor surface expression in confluent endothelial cells. *Blood 117*, 4154−4161.
(33) Spring, K., Chabot, C., Langlois, S., Lapointe, L., Trinh, N. T., Caron, C., Hebda, J. K., Gavard, J., Elchebly, M., and Royal, I. (2012) Tyrosine phosphorylation of DEP-1/CD148 as a mechanism controlling Src kinase activation, endothelial cell permeability, invasion, and capillary formation. *Blood 120*, 2745−2756.
(34) Iuliano, R., Raso, C., Quintiero, A., Le Pera, I., Pichiorri, F., Palumbo, T., Palmieri, D., Pattarozzi, A., Florio, T., Viglietto, G., Trapasso, F., Croce, C. M., and Fusco, A. (2009) The eighth fibronectin type III domain of protein tyrosine phosphatase receptor J influences the formation of protein complexes and cell localization. *J. Biochem. 145*, 377−385.
(35) Atherton, E., and Sheppard, R. C. (1989) *Solid-Phase Peptide Synthesis: A Practical Approach*; IRL Press: Oxford, U.K.
(36) Miranda, L. P., and Alewood, P. F. (1999) Accelerated chemical synthesis of peptides and small proteins. *Proc. Natl. Acad. Sci. U.S.A. 96*, 1181−1186.
(37) Paduano, F., Dattilo, V., Narciso, D., Bilotta, A., Gaudio, E., Menniti, M., Agosti, V., Palmieri, C., Perrotti, N., Fusco, A., Trapasso, F., and Iuliano, R. (2013) Protein tyrosine phosphatase PTPRJ is negatively regulated by microRNA-328. *FEBS J. 280*, 401−412.
(38) Hwang, T. L., and Shaka, A. J. (1995) Water suppression that works. Excitation sculpting using arbitrary wave-forms and pulsed-field gradients. *J. Magn. Reson. 112*, 275−279.
(39) Braunschweiler, L., and Ernst, R. R. (1983) Coherence transfer by isotropic mixing: application to proton correlation spectroscopy. *J. Magn. Reson. 53*, 521−528.
(40) Jenner, J., Meyer, B. H., Bachman, P., and Ernst, R. R. (1979) Investigation of exchange processes by two-dimensional NMR spectroscopy. *J. Chem. Phys. 71*, 4546−4553.
(41) States, D. J., Haberkorn, R. A., and Ruben, D. J. (1982) A two-dimensional nuclear Overhauser experiment with pure absorption phase four quadrants. *J. Magn. Reson. 48*, 286−292.
(42) Bartels, C., Xia, T. H., Billeter, M., Guntert, P., and Wuthrich, K. (1995) The program XEASY for computer-supported NMR spectral analysis of biological macromolecules. *J. Biomol. NMR 6*, 1−10.
(43) Schrödinger LLC, New York, NY., 2010; http://www.schrodinger.com
(44) Mohamadi, F., Richard, N. G. J., Guida, W. C., Liskamp, R., Lipton, M., Caufield, C., Chang, G., Hendrickson, T., and Still, W. C. (1990) MacroModel−an integrated software system for modeling organic and bioorganic molecules using molecular mechanics. *J. Comput. Chem. 11*, 440−467.
(45) McDonald, D. Q., and Still, W. C. (1992) AMBER* Torsional Parameters for the Peptide Backbone. *Tetrahedron Lett. 33*, 7743−7746.
(46) Still, W. C., Tempczyk, A., Hawley, R. C., and Hendrickson, T. (1990) Semianalytical treatment of solvation for molecular mechanics and dynamics. *J. Am. Chem. Soc. 112*, 6127−6129.
(47) Daura, X., Gademann, K., Jaun, B., Seebach, D., Van Gunsteren, W. F., and Mark, A. E. (1999) Peptide folding: When simulation meets experiment. *Angew. Chem., Int. Ed. 38*, 236−240.
(48) Alcaro, S., Gasparrini, F., Incani, O., Mecucci, S., Misiti, D., and Pierini, M. (2000) A "quasi-flexible" automatic docking processing for studying stereoselective recognition mechanisms. Part I. Protocol validation. *J. Comput. Chem. 21*, 515−530.
(49) Alcaro, S., Gasparrini, F., Incani, O., Caglioti, L., Pierini, M., and Villani, C. (2007) ″Quasi flexible″ automatic docking processing for studying stereoselective recognition mechanisms, part 2: Prediction of $\Delta\Delta G$ of complexation and ^{1}H-NMR NOE correlation. *J. Comput. Chem. 28*, 1119−1128.